Lost surface waves in nonpiezoelectric solids

Eugene A. Eliseev,[1] Anna N. Morozovska,[2,3,*] Maya D. Glinchuk,[1] and Sergei V. Kalinin[4,†]

[1]*Institute for Problems of Materials Science, National Academy of Sciences of Ukraine, 3 Krjijanovskogo, 03142 Kyiv, Ukraine*

[2]*Institute of Physics, National Academy of Sciences of Ukraine, 46 Prospekt Nauky, 03028 Kyiv, Ukraine*

[3]*Bogolyubov Institute for Theoretical Physics, National Academy of Sciences of Ukraine, 14-b Metrolohichna Street, 03680 Kyiv, Ukraine*

[4]*Center for Nanophase Materials Science, Oak Ridge National Laboratory, Oak Ridge, Tennessee 37831, USA*

(Received 5 January 2017; revised manuscript received 30 May 2017; published 11 July 2017)

The existence of shear surface acoustic waves (SAWs) has been regarded as impossible in nonpiezoelectrics with homogeneous flat surfaces. We show that transverse shear SAWs can propagate near the flat surfaces of all crystalline dielectrics due to the omnipresent flexoelectric coupling. It appears that the penetration depth of the previously unexplored SAW is defined by the flexocoupling strength. Since the SAW occurs due to the flexoelectric coupling, we name it the flexoelectric SAW (flexo-SAW). We predict that the phonon spectra corresponding to the flexo-SAWs and bulk phonon modes can be separated in thin nonpiezoelectric films, such as strontium titanate.

DOI: 10.1103/PhysRevB.96.045411

I. INTRODUCTION

A. Dynamics at the surfaces of solids

The physical processes taking place at the surface of solids are so versatile that they have become an inexhaustible subject of fundamental research [1,2]. In particular, since the discovery of surface waves in solids [3], they have attracted the increasing attention of scientists [4,5], because experimental and theoretical studies of them can serve as the source of unique information about the surface impact on the dynamics and structure of atomic lattice [6], structural instabilities, and phase transitions induced by the surface [7], and with them the properties of phonons in spatially confined systems [8,9] can be explored. In addition to the fundamental aspects, the surface oscillations and waves are indispensable for applications in modern nanoacoustics [10] and nanoplasmonics [11].

B. Surface waves: From discovery to now

The existence of surface acoustic waves (SAWs) in solids of arbitrary symmetry (including the isotropic one) had been predicted at the end of the 19th century by Lord Rayleigh [3]. The main conclusion made from the Rayleigh solution is that the shear surface wave cannot propagate along the flat surface. The longitudinal-transverse Rayleigh waves are a mixture of shear and dilatation waves of expansions and compressions, in contrast to the acoustic waves propagating in the bulk of a solid matter, which have two transverse shear modes and a longitudinal dilatational one [12]. Only at the end of the 1960s had Bleustein [13] and Gulyaev [14] shown that purely shear surface waves can propagate in some solids without an inversion center (e.g., at definite crystallographic cuts of piezoelectrics), and naturally their appearance is impossible in all nonpiezoelectrics with a homogeneous flat surface. Nonlinear Rayleigh waves propagating along the flat surface of a homogeneous solid medium covered by a thin film were considered in 1998 by Eckl *et al.* [15]. The influence of standing SAWs on the diffusion of an adatom was theoretically studied in 2011 by Taillan *et al.* [16]. Recently interest in the theoretical consideration of classical linear SAWs was renewed by Romero [17], who considered several types of SAWs in piezoelectrics with an ideal flat surface.

Notably, if the surface is not flat the shear waves can appear. In particular, Auld and Gagnepain [18] revealed that any periodic corrugation of the surface (including a very shallow one) leads to shear surface waves. Furthermore, Love waves [12,19] are shear surface waves of a planar substrate coated with a thin layer. The appearance of shear surface waves for a planar substrate supporting an array of mechanical resonators has been reported [20]. Hence one can readily imagine the situation that the observation of shear SAWs at the surface of a nonpiezoelectric will be attributed to surface corrugation [18], artificial inhomogeneities [20], or additional layers [19]. However, in the latter case, SAWs are possible only for a certain ratio between the elastic modules of the layer and the substrate [19]. The conditions for the existence of shear SAWs on corrugated surfaces essentially depend on the form of the inhomogeneity [18]; they are far from being omnipresent. Running ahead, the aim of this work is to show that for the flat surface of an arbitrary solid body (including an isotropic one in the sense of elastic properties) the localization of transverse acoustic waves is always possible under the influence of the omnipresent flexoelectric effect, including the case when all previous theories predicted the complete absence of transverse SAWs.

C. Experimental observations of SAWs

The questions of how to investigate experimentally SAWs and how to verify existing theoretical predictions [13–17], along with many others, naturally arise. Since the frequency of the soft-mode-related optic and acoustic phonons in piezoelectric and paraelectric ferroics typically lays within the THz region and corresponding wave vectors are in the range (0.05–5) nm^{-1}, the phonon spectra $\omega(k)$ can be extracted from the inelastic neutron scattering experiments [21–26] by a conventional procedure. Namely each experimental point of the spectra $\omega_i(k_i)$ (e.g., shown in Fig. 2 in Ref. [21]) is defined

*Corresponding author: anna.n.morozovska@gmail.com

†Corresponding author: sergei2@ornl.gov

from the energy position $\hbar\omega_i$ of the inelastic neutron scattering intensity peak measured at fixed wave vector k_i (see, e.g., Fig. 1 in Ref. [21]).

Hamilton *et al.* [27] performed the first experimental demonstration that SAWs in quartz can be probed by diffraction of cold neutrons. Much earlier Soffer *et al.* [28] proposed an optical imaging method for direct observation and study of SAWs at the nonpolar Y cut of piezoelectric $LiNbO_3$ (typical manifestation of Bleustein and Gulyaev waves). Pyrak-Nolte *et al.* [29] made the first direct observation of the new class of elastic interface waves propagating along the discontinuity of a synthetic fracture in aluminum. De Lima, Jr. *et al.* [30] presented the experimental observation of Bloch oscillations, the Wannier-Stark ladder, and Landau-Zener tunneling of SAWs in perturbed grating structures on a solid substrate (in that case the vertical surface displacement has been measured by interferometric methods).

Fine aspects of the SAWs can be explored by Brillouin [11,31,32] and Raman [33,34] scattering, the ultrasonic pulse-echo method [31,32] allowing hypersound spectroscopic measurements, and surface-enhanced Raman scattering based on incomplete internal reflection [35]. Also there are many advanced techniques for SAW observations operating in the GHz range of frequencies, such as laser ultrasonic experiments [36], optical interferometry [37], and surface Brillouin light scattering [38,39]. These methods are mostly relevant for SAW observations up to the (10–100) GHz range; however it is unlikely that they can "see" SAWs in the THz range of frequencies that is typical for proper and incipient inorganic ferroelectrics.

Thus (except for the THz region) the experimental methods of SAW observation are well evolved and precise enough to probe their finest properties and to verify the most sophisticated theoretical predictions.

D. Expected role of flexocoupling on surface waves

It should be noted that the static flexoelectric effect [40–43], consisting of the appearance of polarization due to the strain gradient (direct flexoeffect) and the appearance of strain due to the polarization gradient (converse flexoeffect), was not taken into account in all known theories of SAWs [3,12–17]. The strain induced by the flexoelectric coupling is linearly proportional to the polarization gradient, $u_{ij}^{sf} = -f_{ijkl}(\partial P_k/\partial x_l)$; here f_{ijkl} are the components of the flexocoupling tensor [40–45], and P_k are polarization components. The static flexoelectric effect exists in all solids, as allowed by arbitrary symmetry, and its strength can be small, moderate, or giant, because f_{ijkl} ranges from (0.1–1) volts [41–45] to hundreds of volts [44].

Moreover the notion of the dynamic flexoelectric effect [43,45,46], consisting of the appearance of polarization P_i^{df} in response to accelerated motion of the medium in the time domain, and its impact on phonon spectra has been absent until recently [47,48]. The dynamic flexoelectric effect was first introduced by Tagantsev [43,49] as $P_i^{df} = -M_{ij}(\partial^2 U_j/\partial t^2)$, where U_j is an elastic displacement and M_{ij} is a flexodynamic tensor.

Nevertheless, an elastic wave of any kind is inevitably accompanied by a periodic gradient of mechanical strain and stress. This gradient is proportional to the wave vector of the oscillation and is obviously small for longer wavelengths. For a medium of arbitrary symmetry (including an isotropic one) the wave of the strain gradient will cause a wave excitation of electric polarization (i.e., the local polarization, the mean value of which is zero) due to the direct flexoelectric effect. The latter, in turn, will affect the elastic stresses associated with the wave due to the converse flexoelectric effect. Thus the flexocoupling should influence the properties of surface waves in all solids, since it essentially affects the bulk phonon spectra in different ferroelectrics and paraelectrics [46–49], and the influence should be more pronounced for shorter wavelengths.

E. Research motivation, impact, and methods

Recently using the Landau-Ginzburg-Devonshire (LGD) phenomenological continuum media approach Morozovska *et al.* [47,48] demonstrated the significant influence of the flexocoupling on the appearance of spatially modulated phases and on the properties of optic and acoustic phonons in the ferroelectric and paraelectric phases of ferroelectrics $PbTiO_3$ and $Sn_2P_2(S,Se)_6$, and paraelectric $SrTiO_3$. Motivated by these results we used the LGD approach for SAW description in paraelectrics. We revealed that the surface shear waves similar to the waves of Bleustein [13] and Gulyaev [14] can exist in dielectrics of any symmetry (e.g., in paraelectric $SrTiO_3$) and for an arbitrary orientation of the surface due to the flexoelectric coupling. The wave is the oscillation of shear strain coupled with electric polarization. Below we classify these types of waves as "flexocoupling-induced SAWs" (briefly as "flexo-SAWs").

Note that previously known types of SAWs (see, e.g., Refs. [12–19]) have been revealed within the phenomenological continuum media approach. We emphasize that our choice of the phenomenological LGD approach conditions the generality of the obtained results, and it shows that the predicted flexo-SAWs exist for all nonpiezoelectric solids, whereas microscopic *ab initio* approaches are material specific.

II. STATEMENT OF THE PROBLEM ALLOWING FOR FLEXOCOUPLING

LGD expansion of bulk (F_V) and surface (F_S) parts of the Helmholtz free energy F on the polarization vector (P_i) and strain tensor components (u_{ij}) has the form [47,48]

$$F_V = \int_V d^3r \left(\frac{a_{ij}}{2} P_i P_j + \frac{a_{ijkl}}{4} P_i P_j P_k P_l - P_i E_i + \frac{g_{ijkl}}{2} \left(\frac{\partial P_i}{\partial x_j} \frac{\partial P_k}{\partial x_l} \right) - q_{ijkl} u_{ij} P_k P_l - \frac{f_{ijkl}}{2} \left(P_k \frac{\partial u_{ij}}{\partial x_l} - u_{ij} \frac{\partial P_k}{\partial x_l} \right) + \frac{c_{ijkl}}{2} u_{ij} u_{kl} + \frac{v_{ijklmn}}{2} \left(\frac{\partial u_{ij}}{\partial x_m} \frac{\partial u_{kl}}{\partial x_n} \right) \right), \tag{1a}$$

$$F_S = \int_S d^2r \frac{a_{ij}^S}{2} P_i P_j. \tag{1b}$$

The components of tensor a_{ij} are positively defined constants for linear dielectrics and explicitly depend on temperature T for ferroelectrics and paraelectrics. In particular, a Barrett-type [50] formula $a_{ij} = \alpha_{ij}^T[T_q \coth(T_q/T) - T_C]$ is valid for incipient paraelectrics like $SrTiO_3$, wherein α_{ij}^T are the inverse Curie-Weiss constants, T_C is the Curie temperature, and T_q is a characteristic temperature. All other tensors in the free energy (1) are supposed to be temperature independent. Tensor a_{ijkl} should be positively defined for the functional stability in paraelectrics and ferroelectrics; it can be neglected for linear dielectrics. Tensors g_{ijkl} and v_{ijklmn}, which determine the magnitude of the gradient energy, are also regarded positively defined. Coefficients q_{ijkl} are the components of electrostriction tensor; c_{ijkl} are the components of the elastic stiffness tensor. Polarization is conjugated with electric field E_i that can include external and depolarization contributions (if any exist). The flexoelectric energy is written in the form of the Lifshitz invariant, $\frac{f_{ijkl}}{2}(P_k \frac{\partial u_{ij}}{\partial x_l} - u_{ij} \frac{\partial P_k}{\partial x_l})$, where f_{ijkl} is the flexocoupling stress tensor.

The Lagrange function is

$$L = \int_t dt(F - K), \tag{2}$$

where the kinetic energy K is given by the expression [43,45,47,49]

$$K = \int_V d^3r \left[\frac{\mu}{2} \left(\frac{\partial P_i}{\partial t} \right)^2 + M_{ij} \frac{\partial P_i}{\partial t} \frac{\partial U_j}{\partial t} + \frac{\rho}{2} \left(\frac{\partial P_i}{\partial t} \right)^2 \right], \tag{3}$$

which includes the dynamic flexoelectric coupling tensor M_{ij}. U_i is the elastic displacement and ρ is the density of a material. The strain components are related to the displacement derivatives in a conventional way, $u_{ij} = \frac{1}{2}(\frac{\partial U_i}{\partial x_j} + \frac{\partial U_j}{\partial x_i})$.

Dynamic equations of state have the form of Euler-Lagrange (E-L) equations:

$$\frac{\delta L}{\delta P_i} = -\Gamma \frac{\partial P_i}{\partial t}, \quad \frac{\delta L}{\delta U_i} = 0. \tag{4}$$

For most of the cases one can neglect the polarization relaxation by setting $\Gamma = 0$ and omit the high-order elastic strain gradient by setting $v_{ijklmn} = 0$, if the flexoelectric coefficients are below the critical values f_{ijkl}^{cr} [51,52]. For the flexoelectric coefficients higher than the critical ones the spatially modulated phase occurs [48], at which the relationship $f_{ijqs}^{cr} f_{klqs}^{cr} \cong g_{ijmn} c_{klmn}$ is valid under the condition $v_{ijklmn} = 0$ [48,51,52].

Hereinafter we regard that the dynamic flexoeffect tensor is diagonal, $M_{ij} = M\delta_{ij}$, and the inequality $M^2 < \rho\mu$ should be valid for the stability of kinetic energy [see Eq. (3)]. Below we use an isotropic approximation for the tensor coefficients $a_{ij}^S = \alpha_{S0}\delta_{ij}$ and $a_{ij} = \alpha(T)\delta_{ij}$, where α_{S0} is the surface energy coefficient, $\alpha(T) = \alpha_T[T_q \coth(T_q/T) - T_C]$, and δ_{ij} is the Kronecker-delta symbol.

The boundary conditions at the mechanically free surface can be obtained from the variation of the free energy (1) on polarization and strain:

$$g_{kjim} n_k \frac{\partial P_m}{\partial x_j} + \alpha_{S0} P_i = -\frac{f_{jkim}}{2} u_{jk} n_m \Big|_S, \quad \sigma_{ij} n_j \big|_S = 0. \tag{5}$$

Here n_k are the components of the external normal to the surface; the elastic stress tensor $\sigma_{ij} = -\delta F_V/\delta u_{ij}$ satisfies the mechanical equilibrium equation, $\partial\sigma_{ij}/\partial x_j = 0$. The most evident consequence of the flexocoupling is the inhomogeneous terms in the boundary conditions (5).

Note that the application of the LGD-type continuum theory for the description of acoustic phonon dispersion for long enough waves with wave vectors $k < 1\,\mathrm{nm}^{-1}$ does not require any special justifications as it is widely used in the literature (see e.g., Refs. [12–17,19,31–35,47,48] and paragraph 3.2 in Ref. [49]), and the results obtained from LGD theory agree well with experimentally measured phonon spectra [31–35,48]. For shorter waves with $k > 1\,\mathrm{nm}^{-1}$ the results presented below have only qualitative significance, but we hope that semiquantitative description of the SAWs can be sufficient to stimulate the search of their experimental verification.

III. ANALYTICAL SOLUTION FOR A LOST SURFACE WAVE

A. Explicit form of the Euler-Lagrange boundary problem for transverse surface waves

Let us consider the transverse wave of electric polarization $P_2(x_1,x_3,t)$ and elastic displacement $U_2(x_1,x_3,t)$ propagating along direction x_1 near the surface $x_3 = 0$ of a semi-infinite nonpiezoelectric solid (see Fig. 1). The wave is not damped by the influence of depolarizing effects because $\mathrm{div}\vec{P}(x_1,x_3,t) = 0$.

The explicit form of the E-L equations (4) for the purely transverse surface waves with the boundary conditions at the surface $x_3 = 0$ is derived in Appendix A of the Supplemental Material [53]. These equations can be linearized in dielectrics and paraelectrics (i.e., at $\alpha > 0$). For the considered geometry the linearized E-L equations along with the boundary conditions (5) acquire relatively simple form (compare with the

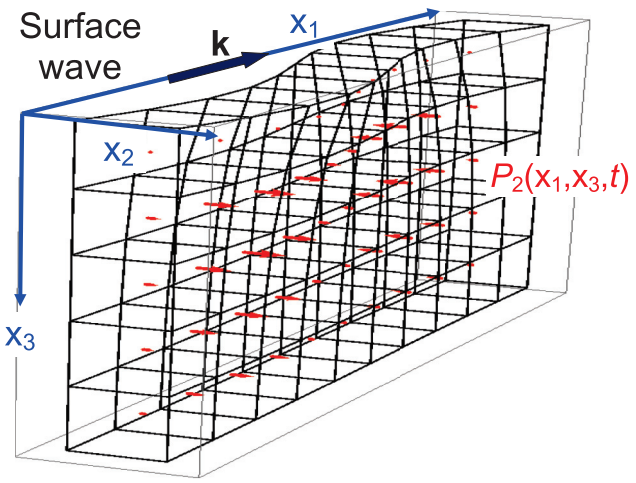

FIG. 1. Geometry of the surface wave propagating in a semi-infinite nonpiezoelectric (dielectric or paraelectric) material. Red arrows are the elementary dipoles, which are zero at the surface in the particular case $\alpha_{S0} = \infty$ [because $P_2(x_1,0,t) = 0$ at $\alpha_{S0} = \infty$]. Black grid illustrates the deformation of the unit cells caused by the displacement $U_2(x_1,x_3,t)$ (the scale is distorted).

equations in paragraph 3.2 in Ref. [49]):

$$\rho\frac{\partial^2 U_2}{\partial t^2}+M\frac{\partial^2 P_2}{\partial t^2}-\Delta(c_{44}U_2+f_{44}P_2)=0, \quad (6a)$$

$$\mu\frac{\partial^2 P_2}{\partial t^2}+M\frac{\partial^2 U_2}{\partial t^2}+\alpha P_2-\Delta(g_{44}P_2+f_{44}U_2)=0. \quad (6b)$$

The symbol Δ stands for the Laplace operator. Boundary conditions (5) acquire the form

$$\left(c_{44}\frac{\partial U_2}{\partial x_3}+f_{44}\frac{\partial P_2}{\partial x_3}\right)\Big|_{x_3=0}=0,$$

$$\left(\alpha_{S0}P_2-g_{44}\frac{\partial P_2}{\partial x_3}-f_{44}\frac{\partial U_2}{\partial x_3}\right)\Big|_{x_3=0}=0. \quad (6c)$$

Hereinafter the inequality $f_{44}^2 < c_{44}g_{44}$ is regarded as valid for the system stability.

B. General expressions relating the amplitudes, frequency dispersion, and penetration depth of the traveling surface waves

Let us look for the solution of the linearized boundary problem (6) in the form of a traveling surface wave:

$$P_2(x_1,x_3,t)=\exp[i(kx_1-\omega t)-\xi x_3]\tilde{p}(k),$$
$$U_2(x_1,x_3,t)=\exp[i(kx_1-\omega t)-\xi x_3]\tilde{u}(k). \quad (7)$$

Here k is the wave vector in the direction of the wave propagation, ω is its frequency, and ξ is inverse penetration depth of the wave. Since the solid occupies the semispace $x_3 \geqslant 0$, only the exponents either vanishing or not increasing at $x_3 \to \infty$ are present, so that the inequality $\mathrm{Re}(\xi) \geqslant 0$ should be valid.

The substitution of expressions (7) in Eqs. (6) leads to the system of linear algebraic equations for the amplitudes $\tilde{p}$ and $\tilde{u}$:

$$[\rho\omega^2+c_{44}(\xi^2-k^2)]\tilde{u}+M\omega^2\tilde{p}+f_{44}(\xi^2-k^2)\tilde{p}=0,$$
$$[\mu\omega^2-\alpha+g_{44}(\xi^2-k^2)]\tilde{p}+M\omega^2\tilde{u}+f_{44}(\xi^2-k^2)\tilde{u}=0. \quad (8)$$

The condition of the system (8) zero determinant gives the condition of the SAW existence

$$[\rho\omega^2+c_{44}(\xi^2-k^2)][\mu\omega^2-\alpha+g_{44}(\xi^2-k^2)]=[M\omega^2+f_{44}(\xi^2-k^2)]^2. \quad (9)$$

The solution of Eq. (9) for the penetration depth of the wave is

$$\xi_{1,2}^2=k^2+\frac{-B(\omega)\pm\sqrt{B^2(\omega)-4[c_{44}g_{44}-(f_{44})^2]C(\omega)}}{2(c_{44}g_{44}-(f_{44})^2)}, \quad (10a)$$

wherein the functions $B(\omega)$ and $C(\omega)$ are given by expressions

$$B(\omega)=(\mu\omega^2-\alpha)c_{44}+\rho\omega^2 g_{44}-2M\omega^2 f_{44}, \quad (10b)$$
$$C(\omega)=\rho\omega^2(\mu\omega^2-\alpha)-(M\omega^2)^2. \quad (10c)$$

The conditions $c_{44}^2R^2(k) \geqslant 4(\rho\omega^2-c_{44}k^2)^2$ and $\frac{(c_{44}\mu+g_{44}\rho-2M f_{44})\omega^2-\alpha(T)c_{44}}{(c_{44}g_{44}-f_{44}^2)}-2k^2<0$ are required for $\mathrm{Re}(\xi_i) \geqslant 0$.

Substitution of the solution (7) rewritten in the explicit form $Q_2=[q_1\exp(-\xi_1x_3)+q_2\exp(-\xi_2x_3)]\exp[i(kx_1-\omega t)]$ (where the symbol $q=p$ for polarization P or $q=u$ for the strain field U) into Eqs. (8) and boundary conditions (6c) leads to the two independent equations for the penetration depths ξ_i:

$$\xi_1=\xi_2, \quad (11a)$$

$$\alpha_{S0}(\rho\omega^2-c_{44}k^2-c_{44}\xi_1\xi_2)=(\xi_1+\xi_2)\xi_1\xi_2[c_{44}g_{44}-(f_{44})^2]. \quad (11b)$$

Along with Eqs. (11) the following relation between the amplitudes p and u should be valid:

$$u_i=-\left(\frac{M\omega^2+f_{44}(\xi_i^2-k^2)}{\rho\omega^2+c_{44}(\xi_i^2-k^2)}\right)p_i. \quad (12)$$

If the shear strain wave is excited by polarization, its resonant enhancement at definite frequency ω is possible under the condition $\rho\omega^2(k)+c_{44}\{\xi_i^2[k,\omega(k)]-k^2\}=0$. The dispersion law $\omega(k)$ will be derived and analyzed below.

The evident form of Eq. (11a) is equivalent to the condition of the zero determinant in Eq. (10a), namely

$$B^2(\omega)-4C(\omega)[c_{44}g_{44}-(f_{44})^2]=0. \quad (13)$$

Note that the solution of Eq. (13) with respect to frequency is independent of the wave vector. A solution with a similar property was found by Romeo *et al.* [17], who noted that for this case the "frequency dispersion" is limited to the discrete set of frequency values $\omega_n(k_n)$, which is unlikely to be observed.

Really in the secular case $\xi_1=\xi_2=\xi$ [Eq. (11a)] the expressions (7) for the solution should be modified as $P_2=(p_1-p_2\xi x_3)\exp[i(kx_1-\omega t)-\xi x_3]$ and $U_2=(u_1-u_2\xi x_3)\exp[i(kx_1-\omega t)-\xi x_3]$. A detailed consideration of the secular case, presented in part D of the Supplemental Material [53], leads to the conclusion that the surface wave can exist under the validity of a very specific boundary condition, $\alpha_{S0}=0$. Since it exists for a definite frequency, the solution (11a) is the "isolated" point that is unlikely to be observed experimentally.

C. Impact of the boundary conditions for polarization on the surface waves' existence

In contrast to the pessimistic scenario of the experimental verification of the secular case (11a), the solution of Eq. (11b) is valid at all values of α_{S0} and can be simplified for two limiting cases, $\alpha_{S0}=0$ and $\alpha_{S0}=\infty$, considered below.

(a) The "bulklike" case I corresponds to the natural boundary condition for polarization at the surface, which is the zero normal derivative, $\partial P_2/\partial x_3|_{x_3=0}=0$, since $\alpha_{S0}=0$. Mathematically case I is equivalent to the condition $\xi_1\xi_2=0$, because $\xi_1+\xi_2\neq 0$. Setting $\xi=0$ in Eq. (9) we immediately obtain the dispersion relation

$$(\rho\omega^2-c_{44}k^2)(\mu\omega^2-\alpha-g_{44}k^2)=(M\omega^2-f_{44}k^2)^2. \quad (14)$$

In fact Eq. (14) represents the dispersion relation for a transverse phonon mode in the bulk, because its decay factor ξ given by Eqs. (10) is zero. As anticipated Eq. (14) coincides

with Eq. (13b) from Ref. [47] in a paraelectric phase with $P_S = 0$ and $2\alpha \to \alpha$ (due to the absence of factor 1/2 in the free energy in Ref. [47]).

(b) The SAW case II corresponds to zero polarization at the surface, $P_2(x_1,0,t) = 0$, since $\alpha_{S0} = \infty$ and thus $\rho\omega^2 - c_{44}k^2 - c_{44}\xi_1\xi_2 = 0$ from Eq. (11b). The latter condition jointly with the condition $p_1 = -p_2$ is sufficient to satisfy the boundary conditions (6c). The dispersion relation obtained from Eqs. (11b) and (10a) is

$$\frac{(\rho\omega^2 - c_{44}k^2)^2}{c_{44}^2} = \frac{(\rho\omega^2 - c_{44}k^2)(\mu\,\omega^2 - \alpha - g_{44}k^2) - (M\,\omega^2 - f_{44}k^2)^2}{c_{44}g_{44} - (f_{44})^2}. \tag{15}$$

The most important point is that under the absence of static ($f_{44} = 0$) and dynamic ($M = 0$) flexocoupling the dispersion relation (15) reduces to the bulk dispersion law, $\rho\omega^2 = c_{44}k^2$, excluding the separate frequency point $\frac{\rho\omega^2}{c_{44}} = \frac{\mu\,\omega^2 - \alpha}{g_{44}}$. In the presence of flexoelectric coupling the explicit form of Eq. (15) is a biquadratic equation

$$A(k)\omega^4 - Q(k)\omega^2 + \frac{\alpha c_{44}k^2}{c_{44}g_{44} - f_{44}^2} = 0, \tag{16a}$$

where the functions $Q(k) = \frac{\alpha\rho}{c_{44}g_{44} - f_{44}^2} + (\frac{g_{44}\rho + c_{44}\mu - 2M\,f_{44}}{c_{44}g_{44} - f_{44}^2} - 2\frac{\rho}{c_{44}})k^2$ and $A(k) = \frac{\rho\mu - M^2}{c_{44}g_{44} - f_{44}^2} - \frac{\rho^2}{c_{44}^2}$ are introduced. Since $c_{44}g_{44} > f_{44}^2$ for the system stability, and $\alpha > 0$ for dielectrics and paraelectrics, the last term in Eq. (16a) is positive for the these materials. Since we regard that $\rho\mu > M^2$ for the Lagrangian (2) stability, the first term $A(k)$ can be of arbitrary sign, but inevitably becomes positive under the condition $f_{44}^2 \to c_{44}g_{44}$, i.e., when the flexoelectric coefficient increases towards the critical value. Under the condition $Q(k) > 0$ and relatively high f_{44}^2 Eq. (16a) has two roots, a transverse optic (TO) and acoustic (TA) mode. At $Q(k) < 0$ and $A(k) < 0$ it contains only one TA mode. The corresponding equation for the decay factors can be derived from Eqs. (9) and (10), namely,

$$\xi^4 + R(k)\xi^2 + \frac{(\rho\omega^2 - c_{44}k^2)^2}{c_{44}^2} = 0, \tag{16b}$$

where the function $R(k) = \frac{(c_{44}\mu + g_{44}\rho - 2M\,f_{44})\omega^2 - \alpha(T)c_{44}}{(c_{44}g_{44} - f_{44}^2)} - 2k^2$ is introduced. Since the last term in Eq. (16b) is positive because of $c_{44}g_{44} > f_{44}^2$, the conditions for which both decay factors ξ_i become real are $R(k) < 0$ and $c_{44}^2R^2(k) \geqslant 4(\rho\omega^2 - c_{44}k^2)^2$. Both ξ_i are complex in the case $c_{44}^2R^2(k) < 4(\rho\omega^2 - c_{44}k^2)^2$, and purely imaginary under the conditions $c_{44}^2R^2(k) \geqslant 4(\rho\omega^2 - c_{44}k^2)^2$ and $R(k) > 0$.

Expressions (13)–(16) are the formal analytical solution of the considered problem, but only Eqs. (16) [being the explicit form of Eq. (15)] contain the "lost" transverse surface wave induced by the flexoelectric coupling, which we abbreviate as flexo-SAWs below. The existence of flexo-SAWs is not limited to a particular material, but for the sake of concreteness, we have chosen a well-studied quantum paraelectric $SrTiO_3$ (STO) for which the majority of constants are known. Below we explore the wave dispersion in a transverse direction and its penetration under the STO surface.

IV. FLEXOCOUPLING IMPACT ON SURFACE WAVE PROPERTIES IN NONPIEZOELECTRIC SOLIDS

A. Frequency dispersion, phase velocity, and penetration depth of SAWs in $SrTiO_3$

Using Eqs. (16) we calculated the frequency dispersion $\omega(k)$ of the traveling wave vector for the case of paraelectric STO at temperatures (100–400) K. TA and TO modes penetrating in the bulk were calculated from Eq. (14). Most of STO material parameters are well known. Numerical values of the unknown STO parameters have been extracted from the fitting [48] of phonon spectra obtained from the inelastic neutron scattering [21]. STO parameters are listed in Table I. Using the parameters and the detectable limit of displacement fluctuation

TABLE I. Description, dimension, and numerical values of parameters in Eqs. (16) collected from Refs. [54–57].

Description of the physical parameter	Symbol and dimension	Numerical value for $SrTiO_3$	Refs.
Coefficient at P^2	$\alpha(T)$ ($\times$C^{-2} m J)	$\alpha_T[T_q\coth(T_q/T) - T_C]$	[50]
Inverse Curie-Weiss constant	α_T ($\times 10^5$ C^{-2} m J/K)	15	[54–57]
Curie temperature	T_C (K)	30	[54–57]
Characteristic temperature	T_q (K)	54	[54–57]
Surface energy coefficient	α_{S0} ($\times$C^{-2} J)	∞	N/A
LGD coefficient at P^4	β ($\times 10^8$ J C^{-4} m^5)	81	[54–57]
LGD coefficient at P^6	γ ($\times 10^9$ J C^{-6} m^9)	0	[54–57]
Electrostriction coefficient	q_{44} ($\times 10^9$ J m/C^2)	2.4	[54,57]
Elastic stiffness coefficient	c_{44} ($\times 10^{10}$ Pa)	11	[54–57]
Gradient coefficient at $(\nabla p)^2$	g_{44} ($\times 10^{-10}$ C^{-2} m^3 J)	0.5 (fitting parameter)	[48]
Elastic strain gradient $(\nabla u)^2$	v ($\times 10^{-9}$ V s^2/m^2)	0 (fitting parameter)	This work
Static flexoelectric coefficient	f_{44} (V)	+2.1 (exp. value)	[48]
Dynamic flexoelectric coefficient	M ($\times 10^{-8}$ V s^2/m^2)	-1 (fitting parameter)	[48]
Kinetic coefficient	μ ($\times 10^{-18}$ s^2 m J)	1.45 (fitting parameter)	[48]
Material density at norm. cond.	ρ ($\times 10^3$ kg/m^3)	4.930 at 120 K	Handbook
Lattice constant	a (nm)	$a_x = a_y = a_z = 0.395$ at 120 K	Handbook

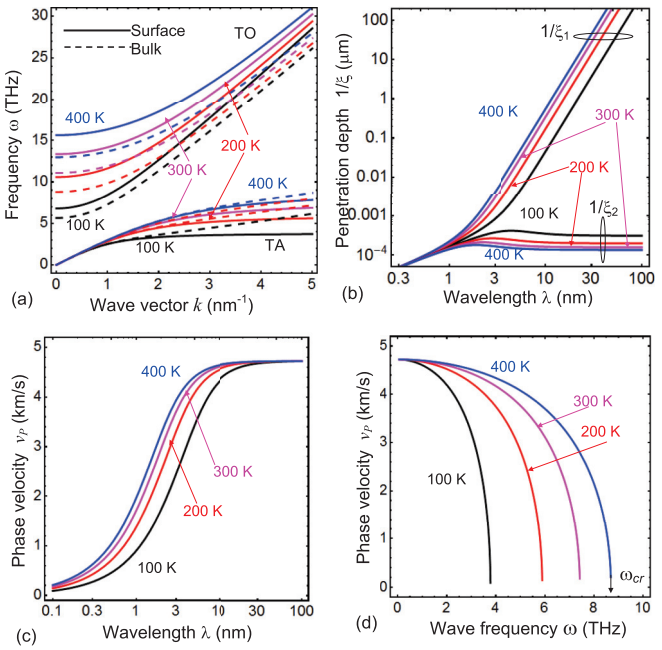

FIG. 2. (a) Frequency dispersion of the bulk (dashed curves) and surface (solid curves) phonon modes calculated for STO parameters. Transverse optic (TO) and acoustic (TA) modes are shown. (b) Dependence of penetration depth of the surface TA wave on its wavelength. (c) Phase velocity of the surface TA wave in dependence on the wavelength. (d) Phase velocity dependence on the surface wave frequency. Different curves in (a)–(d) correspond to the temperatures $T = 100$, 200, 300, and 400 K, which values are specified near the curves. Static flexoelectric coefficient $f_{44} = 2.1$ V, dynamic flexocoupling constant $M = -1 \times 10^{-8}$ V s^2/m^2, surface energy parameter $\alpha_{S0} = \infty$. Other material parameters of STO are listed in Table I.

amplitude $U_2 \sim 1$ pm we obtained the value of polarization amplitude $P_2 \sim 0.05$ C/m^2 from Eq. (12).

The dispersion curves of the lowest transverse acoustic (TA) and transverse optic (TO) surface phonon modes are shown by solid curves in Fig. 2(a). The frequency of TO mode is rather high, and the minimal distance between the TO and TA modes is about 5 THz at $k \approx 1.2$ nm^{-1}. The modes' interaction is very weak in STO, which is typical for paraelectrics. For the sake of comparison the dispersions corresponding to the bulk TA and TO phonon modes are presented by dashed curves in Fig. 2(a). The difference between the dispersion curves for the bulk and surface TO modes is the most pronounced [~(2–5) THz] for small wave vectors $k < 0.5$ nm^{-1} but remains essential for all considered values $0 \leqslant k \leqslant 5$ nm^{-1}. The difference between the frequency dispersion of the bulk and surface TA modes becomes noticeable only for the wave vector values $k > 2$ nm^{-1}. Thus the differences between the bulk and surface TO modes decreases, while the differences between the bulk and surface TA modes increases with the temperature increase [compare solid and dashed curves of different colors in Fig. 2(a)].

Despite that the difference between the frequency dispersions of the surface and bulk TA modes is essentially smaller than between the corresponding TO modes, we further limit our consideration to surface TA mode properties, primarily because their penetration depth is real [Fig. 2(c)] and the acoustic frequency is much lower that the optical one [Fig. 2(a)]. These properties of surface TA modes open the interesting possibilities for their excitation and experimental observation. In contrast, it appeared that TO mode penetration depth is purely imaginary for STO ($\xi = iq_z$) and so it is not localized near the surface. In particular the TO mode calculated from Eqs. (16) is a standing wave reflected from the surface $x_3 = 0$, and it disappears with the flexocoefficient f_{44} decrease below 1.5 V. As a matter of fact the impact of the flexocoupling on the standing TO waves requires a separate study, because their amplitude can be noticeable in thin films (see the next section).

The dependencies of the surface TA wave penetration depths $1/\xi_1$ and $1/\xi_2$ on the wavelength λ are shown in Fig. 2(b) for several temperatures (100–400) K. Because the penetration depth $1/\xi_1$ rapidly increases with the wavelength increase [see solid curves in Fig. 2(b)], the surface wave properties gradually tend to the ones of the bulk wave in the limit $\lambda \to \infty$. The depth $1/\xi_2$ first increases, then reaches a very smooth maximum (or a plateau), and then saturates with the temperature decrease. Both penetration depths $1/\xi_1$ and $1/\xi_2$ almost coincide at small $\lambda < 1$ nm [compare dashed and solid curves in Fig. 2(b)]. Note that the depth $1/\xi_1$ monotonically increases with the temperature increase, and the depth $1/\xi_2$ decreases with the temperature decrease [compare black, red, purple, and blue dashed curves in Fig. 2(b)]. Since the depths determine the localization of the surface wave, only the highest value $1/\xi = \max[1/\xi_1, 1/\xi_2]$ matters.

The dispersion laws for Rayleigh, Bleustein, and Gulyaev waves are similar to those for the bulk elastic (infrasound, acoustic, or ultrasound) waves. Their frequency ω is proportional to the wave number k, namely $\omega = v_P k$, where v_P is the wave velocity. The dependence of the surface TA wave phase velocity $v_P = \omega/k$ on its wavelength $\lambda = 2\pi/k$ is shown in Fig. 2(c) for several temperatures from the range (100–400) K. First the phase velocity increases sharply enough and monotonically with the wavelength increase from 0.1 nm to 10 nm, and then it saturates and tends to the phase velocity of the shear wave in the bulk of material. Smaller v_P values correspond to the lower temperatures [compare black, red, purple, and blue curves in Fig. 2(c)]. The saturation starts at λ values about 5 nm for $T = 400$ K, and about 30 nm for $T = 100$ K.

The frequency spectrum of the phase velocity is shown in Fig. 2(d) for several temperatures (100–400) K. The velocity monotonically decreases with the frequency increase at frequencies less than the critical value ω_{cr}, at which $\omega_{cr} \approx 3.7$ THz at 100 K and $\omega_{cr} \approx 8.75$ THz at 400 K [compare black, red, purple, and blue curves in Fig. 2(d)]. At frequencies $\omega > \omega_{cr}$ the velocity is zero; hence the second-order phase transition occurs at $\omega = \omega_{cr}$. Numerical values of the phase velocity ~ (1–4) km/s are in the same interval as the SAW velocity (3472.5 ± 1.5) m/sec measured by Soffer *et al.* [28] at the nonpolar Y cut of piezoelectric $LiNbO_3$. Soffer waves are typical manifestations of Bleustein and Gulyaev SAWs. However the considered SAWs have the eigenfrequencies $\omega(k) \sim 5$ THz at the wave vectors $k = (1–100)$ nm^{-1}, while the SAWs in $LiNbO_3$ were excited at resonant frequency about 40 MHz at $k = 0.1$ mm^{-1}. The several orders of magnitude difference calls into question the opportunity to observe and

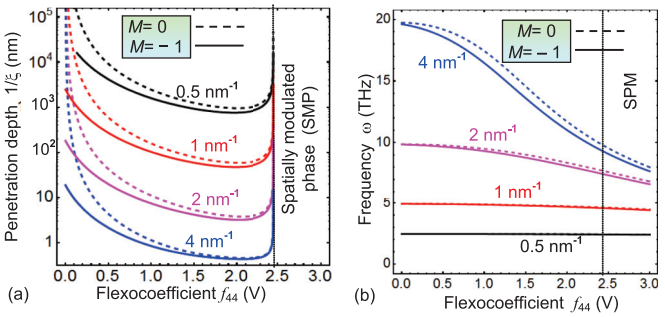

FIG. 3. Dependence of the TA wave penetration depth $1/\xi$ (a) and frequency ω (b) on flexocoefficient f_{44} calculated at 300 K for $M = 0$ (dashed curves) and $M = -1 \times 10^{-8}$ V s^2/m^2 (solid curves). Different curves correspond to the wave vectors $k = (0.5,1,2,4)$ nm^{-1} specified near the curves. STO parameters are listed in Table I.

study flexo-SAWs in paraelectrics using the optical spatial filtering technique [28].

B. Impact of flexocoupling on the SAW frequency dispersion and penetration depth

Note that Fig. 2 is calculated for the static flexoelectric coefficient $f_{44} = 2.1$ V and dynamic flexocoupling constant $M = -1 \times 10^{-8}$ V s^2/m^2 extracted from the soft phonon spectra measured by inelastic neutron scattering (see Fig. 2 in Ref. [21]). Note that the extracted value $f_{44} = 2.1$ V is in surprising agreement with the value $f_{44} = (2.18 \pm 0.05)$ V determined from the bending of the STO crystal by Zubko *et al.* [58], but earlier they measured that $f_{44} = 1.3$ V [59]. The dynamic flexocoupling constant absolute value 1×10^{-8} V s^2/m^2 is within the range (0–20) $\times 10^{-8}$ V s^2/m^2 whose physical reasonability was estimated in Refs. [47,48]. Since exact values of f_{ij} and M are still under debate for most ferroics including ferroelectrics and quantum paraelectrics [60–62], it seems reasonable to explore the properties of the revealed surface TA wave on the value of f_{ij} varying in the actual range (0–3) V. Hereinafter we consider $M < 0$ for STO, because the inequality $M f_{44} < 0$ is in much better agreement with the phonon spectra [21–23] and bending measurements [58] than the case $M f_{44} > 0$. Results are presented in Figs. 3 and 4. The case $M = 0$ is shown in the figures for comparison.

Figure 3(a) shows the dependences of the SAW penetration depth $1/\xi$ on the static flexoelectric coefficient f_{44} calculated for several wave vectors k_n and zero ($M = 0$) and negative ($M < 0$) dynamic flexoconstants. Under the condition $M = 0$ the penetration depth $1/\xi$ sharply increases (up to cm) with the flexoelectric coefficient f_{44} decrease below 0.5 V and diverges when its value tends to zero [see dashed curves in Fig. 3(a)]. When the penetration depth $1/\xi$ diverges, the surface wave properties coincide with the ones of a bulk wave. For wave vectors $k > 1$ nm^{-1} and 1 V $< f_{44} < f_{44}^{cr}$ the TA wave penetration depth $1/\xi$ becomes less than 100 nm, so it indeed becomes a SAW. The depth $1/\xi$ very sharply increases (up to infinity) in the immediate vicinity of $f_{44} \to f_{44}^{cr}$, and becomes imaginary at $f_{44} > f_{44}^{cr}$ indicating the onset of the spatially modulated phase. The critical value of the spatially modulated phase appearance is $f_{44}^{cr} = \sqrt{g_{44}c_{44}} \approx 2.45$ V, and it is independent of the dynamic flexocoupling value as

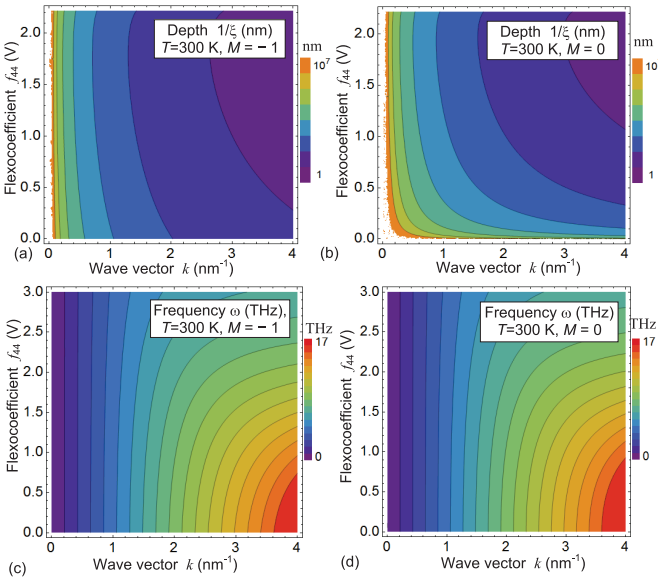

FIG. 4. Contour maps of the TA mode penetration depth $1/\xi$ [(a), (b)] and frequency ω [(c), (d)] in coordinates "wave vector k – flexoelectric coefficient f_{44}" calculated for $T = 300$ K, $M = -1 \times 10^{-8}$ V s^2/m^2 [(a), (c)] and $M = 0$ [(b), (d)]. Parameters corresponding to STO are listed in Table I.

anticipated [48]. The divergence of $1/\xi$ at $f_{44} = 0$ disappears for negative M and positive f_{44}. The corresponding curves have a sharp maximum only at f_{44}^{cr} [see solid curves in Fig. 3(a)]. Actually we established that the divergence $1/\xi$ can originate from the last term $(M\omega^2 - f_{44}k^2)^2$ in Eq. (15) for the TA mode frequency ω. Since the term is positive for the case $f_{44}M < 0$, the corresponding penetration depths given by Eqs. (10) are finite. The negative sign of f_{44} induces the additional divergence of $1/\xi$ at negative M values. At the same time the inequality $M f_{44} > 0$ seems in contradiction with the values extracted from the neutron scattering [22,23] and bending [58] experiments in STO. However the condition $M f_{44} \geqslant 0$ is far from excluded for other materials.

Figure 3(b) shows the dependence of the TA mode frequency ω on the static flexoelectric coefficient f_{44}, calculated for the cases $M = 0$ and $M < 0$, respectively. The difference between these two cases is relatively small [compare the solid and dashed curves in Fig. 3(b)], leading to the conclusion that the impact of the dynamic flexoconstant value on the frequency ω of the surface TA mode is relatively small (at least in comparison with its influence on the penetration depth). For both cases $M = 0$ and $M < 0$ the frequency ω becomes higher than 2.5 THz for small wave vectors $k \geqslant 0.5$ nm^{-1} and flexocoefficients f_{44} lying in the range (0–3) V. The frequency values are relatively high (>4 THz) and almost independent of the flexoelectric coefficient f_{44} for wave vectors $k < 1$ nm^{-1}; they start to decrease slowly with f_{44} increasing for $k > 1$ nm^{-1}. Note that THz values are typical for the soft phonon frequencies in proper and incipient ferroelectrics.

Figures 4(a) and 4(b) demonstrate the dependencies of the SAW penetration depth $1/\xi$ on the flexoelectric coefficient f_{44} and wave vector k calculated for the cases $M = 0$ and $M < 0$, respectively. Under the condition $M = 0$ the penetration

depth $1/\xi$ sharply increases (up to cm) with the flexoelectric coefficient f_{44} decrease below 0.5 V and diverges when its value tends to zero [see different contour lines in Fig. 4(a)]. The divergence of $1/\xi$ at $f_{44} = 0$ disappears for negative M and positive f_{44}. The corresponding curves have a sharp maximum at f_{44}^{cr} only [see different contour lines in Fig. 4(b)].

Figures 4(c) and 4(d) show the dependence of the surface TA mode frequency ω on the flexoelectric coefficient f_{44} and wave vector k calculated for the cases $M = 0$ and $M < 0$, respectively. The difference between these cases is relatively small. For both $M = 0$ and $M < 0$ the frequency ω becomes higher than 1 THz for small wave vectors $k \geqslant 0.2\,\mathrm{nm}^{-1}$ and flexocoefficient $0 < f_{44} < 3\,\mathrm{V}$. The frequency ω is almost independent of f_{44} for wave vectors $k < 1\,\mathrm{nm}^{-1}$ [see almost vertical contour lines of constant ω in Figs. 4(c) and 4(d)]. Under the condition $k > 1\,\mathrm{nm}^{-1}$ the frequency relatively slowly and monotonically decreases with f_{44} increase [Figs. 4(c) and 4(d)].

To resume the analyses of the graphical results presented in Sec. IV we can state that the existence and penetration depth of the revealed surface TA phonon mode is ruled by the static and dynamic flexocouplings. In particular the mode transforms to the bulk wave in the absence of the couplings. So the flexoelectricity indeed generates previously unexplored types of acoustic waves, further abbreviated as flexo-SAWs, which can travel near the flat surface of any solid. Next we can speculate on whether these surface waves be excited and detected separately from the classical bulk phonon modes.

V. POSSIBILITIES OF FLEXO-SAW EXCITATION AND EXPERIMENTAL OBSERVATION

Since the calculated frequency dispersion $\omega(k)$ of the flexo-SAW is within THz region for the wave vectors in the range $k = (0.05\text{–}5)\,\mathrm{nm}^{-1}$ in nonpiezoelectric paraelectrics with relatively small coefficient $\alpha \cong 1/\varepsilon_0\varepsilon$ (corresponding to the high relative dielectric permittivity $\varepsilon \geqslant 100$), the waves can be excited similarly to the bulk acoustic phonons, and the dispersion $\omega(k)$ can be determined from inelastic neutron scattering [21,22]. For instance the dispersion curves of the bulk and surface TO and TA modes in STO are shown in Fig. 5(a) for the actual range of neutron energies ($5\,\mathrm{meV} \leqslant 2\pi\hbar^2k^2/m_n \leqslant 50\,\mathrm{meV}$) and different temperatures ($100\,\mathrm{K} \leqslant T \leqslant 400\,\mathrm{K}$).

We expect that the peaks of inelastic neutron scattering intensity corresponding to the surface and bulk phonon modes can be separated in thin nonpiezoelectric paraelectric layers, where the phonon spectra near the surface becomes more and more important with the thickness decrease, and corresponding peak either splits or shifts. This is possible because the difference between the energy of the surface and bulk phonons is $\Delta E_{TO}(k) = (1\text{–}3)$ meV for TO modes at $k = (0.1\text{–}5)\,\mathrm{nm}^{-1}$, and $\Delta E_{TA}(k) = -(0.5\text{–}3)$ meV for TA modes at $k > 2\,\mathrm{nm}^{-1}$ at temperatures (100–300) K [see Fig. 5(c)]. The corresponding penetration depth of the TA mode $\xi^{-1}(k)$ is about or less than 10 nm at $k > 1\,\mathrm{nm}^{-1}$ and $T = 100\,\mathrm{K}$, and at $k > 2\,\mathrm{nm}^{-1}$ and $T = 300\,\mathrm{K}$ [see Fig. 5(b)]. So we expect that the surface and bulk phonon modes can be separated in thin nonpiezoelectric layers with a thickness of about several penetration depths, which is about or less than 50 nm for STO. In thin layers both surfaces contribute to the response. For a macroscopic sample

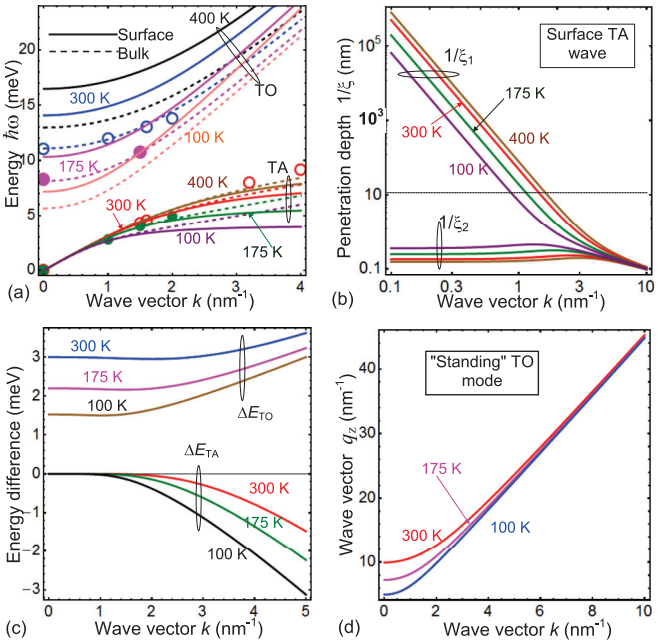

FIG. 5. (a) Energy dispersion $\hbar\omega(k)$ of the bulk (dashed curves) and surface (solid curves) phonon modes calculated in STO. Transverse optic (TO) and acoustic (TA) modes are shown. Symbols are initial experimental data from Fig. 2 in Ref. [21]. (b) Dispersion of the surface TA mode penetration depth $\xi^{-1}(k)$. Different curves in (a) and (b) correspond to the temperatures $T = 100$, 175, 300, and 400 K, which values are specified near the curves. (c) Energy difference $\Delta E(k)$ of the surface and bulk TO modes (top curves with label ΔE_{TO}) and TA modes (bottom curves with label ΔE_{TA}). (d) Dispersion of the TO mode wave vector $q_z(k)$ in the direction x_3, normal to the surface. Corresponding localization depth is purely imaginary, $\xi = iq_z$. Different curves in parts (c) and (d) correspond to the temperatures $T = 100$, 175, and 300 K, which values are specified near the curves. STO parameters obtained from the fitting of experimental data [21] are listed in Table I.

each peak position corresponds to the response of each bulk acoustic or optic mode, which positions are well known for many ferroics and typically tabulated (e.g., for STO).

TO modes, whose "penetration depth" appeared purely imaginary for STO parameters [see Fig. 5(d)], can be imagined as standing TO waves reflected from the surface $x_3 = 0$. As was mentioned, the TO mode disappears with flexocoefficient f_{44} decrease below 1.5 V. The standing TO waves are expected to be noticeable in thin films, whose thickness is an integral multiple of their period $2\pi/q_z(k)$.

The dispersion of the TA shear strain wave amplitudes $u_i(k)$ calculated from Eq. (12) is shown in Fig. 6(a). The amplitude is normalized on the polarization amplitudes p_i regarded proportional to the applied electric field $\mathbf{E}_0$, $p_i \sim \chi_{ij}E_j^0$. Contour maps of amplitudes of polarization $P_2(x_1,x_3,t)$ and displacement $U_2(x_1,x_3,t)$ components in the TA wave are shown in Figs. 6(b) and 6(c), respectively. The maps were calculated from Eq. (7) for fixed frequency $\omega(k)$, time $t = 2\pi/\omega(k)$, and wave vector $k = 1\,\mathrm{nm}^{-1}$. As one can see from Fig. 6(b) the polarization wave is zero at the surface $x_3 = 0$ for the case $\alpha_{S0} = \infty$, because $p_1 = -p_2$. The wave

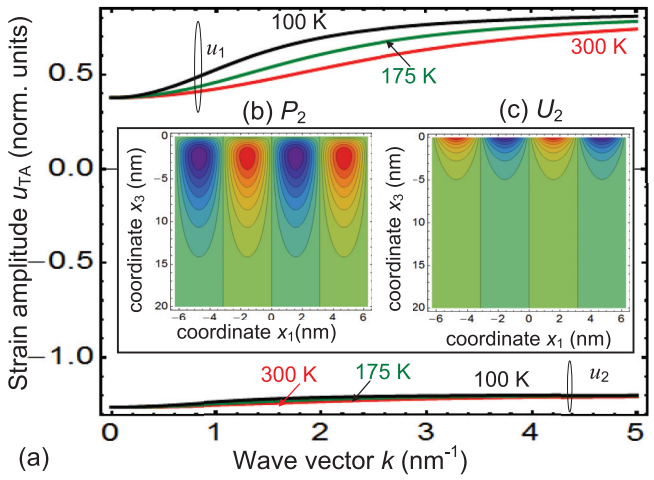

FIG. 6. (a) The dispersion of the normalized TA wave strain amplitudes $u_i[\omega(k),k]$ calculated in STO at temperatures 100, 175, and 300 K, which values are shown near the curves. The amplitude is normalized on the polarization amplitudes p_i. Insets: Contour maps of the TA wave amplitudes $P_2(x_1,x_3,t)$ (b) and $U_2(x_1,x_3,t)$ (c) calculated from Eq. (7) for fixed wave vector $k = 1\,\text{nm}^{-1}$ and time $t = 2\pi/\omega(k)$. STO parameters are listed in Table I.

amplitude has a maximum at depth $x_3 \approx 2\,\text{nm}$ and becomes negligibly small at $x_3 > 15\,\text{nm}$. Displacement is maximal at $x_3 = 0$ and exponentially vanishes at $x_3 > 5$ nm. So the neutron scattering in thin STO films of thickness less than (20–50) nm should give us information about the surface TA phonons coupled with flexoelectricity.

To resume the section, the possibility of flexo-SAW observation by inelastic neutron scattering is much more favorable in thin layers (<50 nm) of paraelectrics and incipient ferroelectrics with dielectric permittivity $\varepsilon \gg 100$ (i.e., in STO or KTO at low temperatures) in comparison with linear low-k dielectrics with $\varepsilon \leqslant 10$. Also we hope that some of the predicted properties of flexo-SAWs can be verified and explored using optical imaging, infrared spectroscopy, Raman and Brillouin scattering, and surface-enhanced Raman scattering based on incomplete internal reflection. Also lattice dynamics calculations (complementary to the LGD approach) could be in order, but unfortunately they are beyond our possibilities.

VI. CONCLUSION

The existence of the shear SAWs was regarded as impossible in nonpiezoelectrics with a flat homogeneous surface without taking into account the flexoelectric coupling. We predict that shear transverse SAWs can propagate in all crystalline dielectrics with the flexoelectric coupling, and name them flexo-SAWs. In particular, we predict that the flexo-SAWs should have rather unusual dispersion properties, whose main features are the following:

(1) The existence and penetration depth of the flexo-SAW is ruled by the static and dynamic flexoelectric couplings. In particular, the penetration depth of the acoustic mode is relatively small (several nm) for moderate and high values of the flexocoupling strength and diverges in the absence of the flexoelectric coupling, and in the latter case these waves become indistinguishable from the bulk waves.

(2) With decreasing the wave vector k the wave velocity along the surface approaches the speed of bulk shear waves, while the penetration depth tends to infinity.

(3) For wavelengths about micrometer order and less the phase velocity of the surface wave decreases, and its penetration depth increases up to tens of microns.

(4) The dispersion relation for flexo-SAWs depends strongly on the boundary conditions for the electric polarization at the surface of the material.

Since the SAW transforms to the bulk wave in the absence of the couplings, we conclude that the flexoelectricity indeed generates previously unexplored types of SAWs, flexo-SAWs, which can travel near the flat surface of any solid. The flexo-SAW has THz frequency in the paraelectric $SrTiO_3$, and its penetration depth varies from nanometers to hundreds of microns depending on the wave vector varying from $0.1\,\text{nm}^{-1}$ to $10\,\text{nm}^{-1}$.

We expect that the peaks of inelastic neutron scattering intensity corresponding to the flexo-SAW and bulk phonon modes can be separated in paraelectric layers of thickness less than (20–50) nm, giving us an independent opportunity to define the flexoelectric coefficients, which are poorly measured by other methods. The absence of the experimental observations of flexo-SAWs can be explained by a very small neutron scattering intensity in thin layers.

In contrast to acoustic modes, it appears that the penetration depth of transverse optic modes is purely imaginary for strontium titanate and so they are not localized near the surface. In fact the mode is a standing wave reflected from the surface, and it disappears with the flexoelectric coefficient decrease. The impact of the flexocoupling on the standing waves deserves a separate theoretical study, because their amplitude can be noticeable in thin paraelectric films.

ACKNOWLEDGMENTS

The authors are grateful to the referees for valuable remarks, suggestions, and help with the literature analysis.

E.A.E. and A.N.M. contributed equally to the research idea, problem statement, and analytical calculations; E.A.E. prepared the graphics, and A.N.M. wrote the manuscript draft. M.D.G. worked intensively on the results analyses and discussion. S.V.K. contributed significantly to the research motivation, results analyses and discussion, manuscript text, and structure improvement.

This manuscript has been authored by UT-Battelle, LLC, under Contract No. DE-AC0500OR22725 with the US Department of Energy. The United States Government retains and the publisher, by accepting the article for publication, acknowledges that the United States Government retains a non-exclusive, paid-up, irrevocable, world-wide license to publish or reproduce the published form of this manuscript, or allow others to do so, for the United States Government purposes. The Department of Energy will provide public access to these results of federally sponsored research in accordance with the DOE Public Access Plan (http://energy.gov/downloads/doe-public-access-plan).

[1] P. G. de Gennes, Wetting: Statics and dynamics, Rev. Mod. Phys. **57**, 827 (1985).

[2] V. A. Shchukin and D. Bimberg, Spontaneous ordering of nanostructures on crystal surfaces, Rev. Mod. Phys. **71**, 1125 (1999).

[3] Lord Rayleigh, On waves propagated along the plane surface of an elastic solid, Proc. London Math. Soc. **s1-17**, 4 (1885).

[4] Z. Yu and S. Boseck, Scanning acoustic microscopy and its applications to material characterization, Rev. Mod. Phys. **67**, 863 (1995).

[5] K. Länge, B. E. Rapp, and M. Rapp, Surface acoustic wave biosensors: A review, Anal. Bioanal. Chem. **391**, 1509 (2008).

[6] M. M. de Lima, Jr. and P. V. Santos, Modulation of photonic structures by surface acoustic waves, Rep. Prog. Phys. **68**, 1639 (2005).

[7] A. N. Alexeyev and D. V. Roshchupkin, Diffraction of surface acoustic waves on the zigzag domain wall in a $Gd_2(MoO_4)_3$ crystal, Appl. Phys. Lett. **68**, 159 (1996).

[8] J. Schiefele, J. Pedrós, F. Sols, F. Calle, and F. Guinea, Coupling Light into Graphene Plasmons through Surface Acoustic Waves, Phys. Rev. Lett. **111**, 237405 (2013).

[9] T. Yukihiro and S.-i. Tamura, Surface acoustic waves in two-dimensional periodic elastic structures, Phys. Rev. B **58**, 7958 (1998).

[10] E. S. K. Young, A. V. Akimov, M. Henini, L. Eaves, and A. J. Kent, Subterahertz Acoustical Pumping of Electronic Charge in a Resonant Tunneling Device, Phys. Rev. Lett. **108**, 226601 (2012).

[11] J.-C. Beugnot, S. Lebrun, G. Pauliat, H. Maillotte, V. Laude, and T. Sylvestre, Brillouin light scattering from surface acoustic waves in a subwavelength-diameter optical fibre, Nat. Commun. **5**, 5242 (2014).

[12] L. D. Landau, E. M. Lifshitz, A. M. Kosevich, and L. P. Pitaevskii, *Theory of Elasticity*, 3rd ed. (Butterworth-Heinemann, Oxford, 1986).

[13] J. L. Bleustein, A new surface wave in piezoelectric materials, Appl. Phys. Lett. **13**, 412 (1968).

[14] Yu. V. Gulyaev, Electroacoustic surface waves in solids, Zh. Eksp. Teor. Fiz., Pis'ma Red. **9**, 63 (1969).

[15] C. Eckl, A. P. Mayer, and A. S. Kovalev, Do Surface Acoustic Solitons Exist? Phys. Rev. Lett. **81**, 983 (1998).

[16] C. Taillan, N. Combe, and J. Morillo, Nanoscale Self-Organization Using Standing Surface Acoustic Waves, Phys. Rev. Lett. **106**, 076102 (2011).

[17] M. Romeo, Surface waves in hexagonal micropolar dielectrics, Int. J. Solids Struct. **87**, 39 (2016).

[18] B. A. Auld and J. J. Gagnepain, Horizontal shear surface waves on corrugated surfaces, Electron. Lett. **12**, 650 (1976).

[19] A. E. H. Love, *Some Problems of Geodynamics* (Cambridge University Press, New York, 1911), p. 144.

[20] A. A. Maznev and V. E. Gusev, Waveguiding by a locally resonant metasurface, Phys. Rev. B **92**, 115422 (2015).

[21] Y. Yasusada and G. Shirane, Neutron scattering and nature of the soft optical phonon in $SrTiO_3$, J. Phys. Soc. Jpn. **26**, 396 (1969).

[22] G. Shirane and Y. Yamada, Lattice-dynamical study of the 110 K phase transition in $SrTiO_3$, Phys. Rev. **177**, 858 (1969).

[23] G. Shirane, J. D. Axe, J. Harada, and J. P. Remeika, Soft ferroelectric modes in lead titanate, Phys. Rev. B **2**, 155 (1970).

[24] J. D. Axe, J. Harada, and G. Shirane, Anomalous acoustic dispersion in centrosymmetric crystals with soft optic phonons, Phys. Rev. B **1**, 1227 (1970).

[25] R. Currat, H. Buhay, C. H. Perry, and A. M. Quittet, Inelastic neutron scattering study of anharmonic interactions in orthorhombic $KNbO_3$, Phys. Rev. B **40**, 10741 (1989).

[26] J. Hlinka, S. Kamba, J. Petzelt, J. Kulda, C. A. Randall, and S. J. Zhang, Origin of the "Waterfall" Effect in Phonon Dispersion of Relaxor Perovskites, Phys. Rev. Lett. **91**, 107602 (2003).

[27] W. A. Hamilton, A. G. Klein, G. I. Opat, and P. A. Timmins, Neutron Diffraction by Surface Acoustic Waves, Phys. Rev. Lett. **58**, 2770 (1987).

[28] D. H. Soffer, D. H. Close, and M. E. Pedinoff, An optical imaging method for direct observation and study of acoustic surface waves, Appl. Phys. Lett. **15**, 339 (1969).

[29] L. J. Pyrak-Nolte, J. Xu, and G. M. Haley, Elastic Interface Waves Propagating in a Fracture, Phys. Rev. Lett. **68**, 3650 (1992).

[30] M. M. de Lima, Jr., Yu. A. Kosevich, P. V. Santos, and A. Cantarero, Surface Acoustic Bloch Oscillations, the Wannier-Stark Ladder, and Landau-Zener Tunneling in a Solid, Phys. Rev. Lett. **104**, 165502 (2010).

[31] A. Kohutych, R. Yevych, S. Perechinskii, V. Samulionis, J. Banys, and Yu. Vysochanskii, Sound behavior near the Lifshitz point in proper ferroelectrics, Phys. Rev. B **82**, 054101 (2010).

[32] K. Z. Rushchanskii, A. Molnar, R. Bilanych, R. Yevych, A. Kohutych, Yu. M. Vysochanskii, V. Samulionis, and J. Banys, Observation of nonequilibrium behavior near the Lifshitz point in ferroelectrics with incommensurate phase, Phys. Rev. B **93**, 014101 (2016).

[33] J. Hlinka, I. Gregora, and V. Vorlicek, Complete spectrum of long-wavelength phonon modes in $Sn_2P_2S_6$ by Raman scattering, Phys. Rev. B **65**, 064308 (2002).

[34] I. Gregora, and J. Hlinka, Directional dispersion of polar optical phonon frequencies in low-symmetry crystals: Raman studies on $Sn_2P_2S_6$, Ferroelectrics **267**, 237 (2002).

[35] G. Dovbeshko, O. Fesenko, A. Dementjev, R. Karpicz, V. Fedorov, and O. Y. Posudievsky, Coherent anti-Stokes Raman scattering enhancement of thymine adsorbed on graphene oxide, Nanoscale Res. Lett. **9**, 263 (2014).

[36] Y. Sugawara, O. B. Wright, O. Matsuda, M. Takigahira, Y. Tanaka, S. Tamura, and V. E. Gusev, Watching Ripples on Crystals, Phys. Rev. Lett. **88**, 185504 (2002).

[37] K. Kokkonen, M. Kaivola, S. Benchabane, A. Khelif, and V. Laude, Scattering of surface acoustic waves by a phononic crystal revealed by heterodyne interferometry, Appl. Phys. Lett. **91**, 083517 (2007).

[38] P. Mutti, C. E. Bottani, G. Ghislotti, M. Beghi, G. A. D. Briggs, and J. R. Sandercock, Surface Brillouin scattering: Extending surface wave measurements to 20 GHz, *Advances in Acoustic Microscopy* (Springer, New York, 1995), pp. 249-300.

[39] A. G. Every, L. M. Kotane, and J. D. Comins, Characteristic wave speeds in the surface Brillouin scattering measurement of elastic constants of crystals, Phys. Rev. B **81**, 224303 (2010).

[40] V. S. Mashkevich and K. B. Tolpygo, The interaction of vibrations of nonpolar crystals with electric fields, Zh. Eksp. Teor. Fiz. **32**, 520 (1957).

[41] Sh. M. Kogan, Piezoelectric effect under an inhomogeneous strain and an acoustic scattering of carriers of current in crystals, Solid State Phys. **5**, 2829 (1963).

[42] A. K. Tagantsev, Piezoelectricity and flexoelectricity in crystalline dielectrics, Phys. Rev. B **34**, 5883 (1986).

[43] P. V. Yudin and A. K. Tagantsev, Fundamentals of flexoelectricity in solids, Nanotechnology **24**, 432001 (2013).

[44] J. Narvaez and G. Catalan, Origin of the enhanced flexoelectricity of relaxor ferroelectrics, Appl. Phys. Lett. **104**, 162903 (2014).

[45] P. Zubko, G. Catalan, and A. K. Tagantsev, Flexoelectric effect in solids, Annu. Rev. Mater. Res. **43**, 387 (2013).

[46] A. Kvasov and A. K. Tagantsev, Dynamic flexoelectric effect in perovskites from first-principles calculations, Phys. Rev. B **92**, 054104 (2015).

[47] A. N. Morozovska, Y. M. Vysochanskii, O. V. Varenyk, M. V. Silibin, S. V. Kalinin, and E. A. Eliseev, Flexocoupling impact on the generalized susceptibility and soft phonon modes in the ordered phase of ferroics, Phys. Rev. B **92**, 094308 (2015).

[48] A. N. Morozovska, E. A. Eliseev, C. M. Scherbakov, and Y. M. Vysochanskii, The influence of elastic strain gradient on the upper limit of flexocoupling strength, spatially modulated phases, and soft phonon dispersion in ferroics, Phys. Rev. B **94**, 174112 (2016).

[49] Edited by A. K. Tagantsev and P. V. Yudin, *Flexoelectricity in Solids: From Theory to Applications* (World Scientific, New Jersey, 2016).

[50] J. H. Barrett, Dielectric constant in perovskite type crystals, Phys. Rev. **86**, 118 (1952).

[51] E. A. Eliseev, A. N. Morozovska, M. D. Glinchuk, and R. Blinc, Spontaneous flexoelectric/flexomagnetic effect in nanoferroics, Phys. Rev. B. **79**, 165433 (2009).

[52] P. V. Yudin, R. Ahluwalia, and A. K. Tagantsev, Upper bounds for flexocoupling coefficients in ferroelectrics, Appl. Phys. Lett. **104**, 082913 (2014).

[53] See Supplemental Material at http://link.aps.org/supplemental/10.1103/PhysRevB.96.045411 for the derivation of the Euler-Lagrange equations.

[54] Y. L. Li, S. Choudhury, J. H. Haeni, M. D. Biegalski, A. Vasudevarao, A. Sharan, H. Z. Ma, J. Levy, V. Gopalan, S. Trolier-McKinstry, and D. G. Schlom, Phase transitions and domain structures in strained pseudocubic (100) $SrTiO_3$ thin films, Phys. Rev. B **73**, 184112 (2006).

[55] A. K. Tagantsev, E. Courtens, and L. Arzel, Prediction of a low-temperature ferroelectric instability in antiphase domain boundaries of strontium titanate, Phys. Rev. B **64**, 224107 (2001).

[56] P. A. Fleury and J. M. Worlock, Electric-field-induced Raman scattering in $SrTiO_3$ and $KTaO_3$, Phys. Rev. **174**, 613 (1968).

[57] N. A. Pertsev, A. K. Tagantsev, and N. Setter, Phase transitions and strain-induced ferroelectricity in $SrTiO_3$ epitaxial thin films, Phys. Rev. B **61**, R825 (2000).

[58] P. Zubko, G. Catalan, A. Buckley, P. R. L. Welche, and J. F. Scott, Erratum: Strain-Gradient-Induced Polarization in $SrTiO_3$ Single Crystals, Phys. Rev. Lett. **100**, 199906 (2008).

[59] P. Zubko, G. Catalan, A. Buckley, P. R. L. Welche, and J. F. Scott, Strain-Gradient-Induced Polarization in $SrTiO_3$ Single Crystals, Phys. Rev. Lett. **99**, 167601 (2007).

[60] A. Biancoli, C. M. Fancher, J. L. Jones, and D. Damjanovic, Breaking of macroscopic centric symmetry in paraelectric phases of ferroelectric materials and implications for flexoelectricity, Nat. Mater. **14**, 224 (2015).

[61] M. Stengel, Unified *ab initio* formulation of flexoelectricity and strain-gradient elasticity, Phys. Rev. B **93**, 245107 (2016).

[62] M. Stengel, Flexoelectricity from density-functional perturbation theory, Phys. Rev. B **88**, 174106 (2013).